

Applied Adaptive Controller Design for Vibration Suppression in Electromagnetic Systems

Zhizhou Zhang

College of Aerospace Science
National University of Defense Technology, Changsha 410073, Hunan, People's Republic of China
zhangzhizhou@nudt.edu.cn

Abstract — In engineering tests, the vehicle-track coupled vibration is very easy to occur on the elastic support beams for a magnetic levitation (maglev) system. The fundamental waves, higher order harmonics, and other components related to the mode of track vibrations are often observed in the gap, acceleration and current sensors. This paper aims to design an adaptive filter to suppress these vibration components and improve the ride comfort for the passengers. Firstly, an adaptive self-turning filter is designed to filter out wideband signals and noise from the original signals, and enhance the strength of the fundamental wave and the harmonic components related to the mode of track vibration. Secondly, a narrow-band bandpass filter is presented to extract these enhanced periodical signals related to the track mode, and then the enhanced signals are configured as the reference inputs of the subsequent adaptive noise canceller. Thirdly, the adaptive noise canceller filters out periodical vibration components related to the track mode. Finally, the designed digital adaptive filter is applied to a real maglev system and suppresses coupled vibration on the elastic support beams effectively.

Index Terms — Adaptive notch filter, magnetic levitation system, noise canceller, self-turning filter, vibration control.

I. INTRODUCTION

Engineering tests show that when as a magnetic levitation (maglev) system is stationary suspension or slowly running on an elastic track, the system can easily induce a coupled vibration between the vehicle and track. These elastic tracks may be the cantilever beams and steel beams outside the garage, or switches in the maintenance platform. The vehicle-track coupled vibration may cause the instability of the maglev system, which directly affects normal operation of maglev train [1,2]. For example, strong vehicle-track coupled vibration occurs in Japan HSST04, German TR04, and US AMT trains [3]. In the process of commercialization of maglev trains, China has encountered similar vibration problem on the elastic beams [4].

In the past studies, in order to avoid the coupled vibration between vehicle and track, the main way is to increase the track stiffness or reduce the static suspension time to avoid the excitation of vibration [3]. Increasing track stiffness will add the system cost while reducing the static suspension time will not fundamentally solved the problem of vehicle-track coupled vibration.

Studies have shown that the vehicle-track coupled vibration is caused by elastic deformation of the track [3]. Thus, the vibration mechanism can be investigated from the perspective of dynamical behavior of maglev system. However, the effect of elastic deformation of the track are rarely taken into account in previous studies [4-6]. They often regard the elastic deformation of the track as 0 to simplify the problem when studying the bifurcation behavior of the maglev system, which is closely related to the vehicle-track coupled vibration. Some researchers have established a five-order system by taking elastic deformation into account [7,8], and preliminarily investigated the Hopf bifurcation type of the complicated system as well as the corresponding periodical solution considering the time delay of the sensors [4-6].

To solve the engineering problem of vehicle-track coupled vibration in maglev systems, several researchers have attempted to suppress vehicle-track coupled vibrations from the perspective of signal processing technology. Zhang [9], Li [10], and Han [11] have designed the band-stop filters or differentiators respectively to suppress the coupled vibration of maglev systems to a certain degree. Zhang [12] designed an FPGA-based gap differentiator with full and rapid convergence, which can suppress vehicle-track coupled vibration on the fixed elastic track but shows poor adaptability to different elastic tracks.

Test results show that when the vehicle-track coupled vibration occurs on beams with different stiffness, the periodical signals with different frequencies appear in the sensor signals. The basic frequencies of this periodical signal are inconsistent and generally distributed in the range of 45 to 60 Hz. The second and third harmonica components are generally distributed in the range of 90 to 120 Hz and 135 to 180 Hz, respectively. An intuitive

hypothesis is that if the periodical signal related to the vibration frequency in the sensor is largely weakened, the vehicle-track coupled vibration may be suppressed significantly.

Because the vibration frequency of periodical signals related to the track mode changes depending on different elastic tracks, those notch filters with fixed central frequency cannot suppress these vibrations with variable frequencies. This paper aims to design an adaptive filter to suppress these vibration components and improve ride comfort for the passengers. An adaptive self-tuning filter is designed to enhance the strength of the fundamental wave and the harmonic components related to the mode of track vibration. And a narrow-band bandpass filter is presented to extract these enhanced periodic signals above and then the enhanced signals are configured as the reference inputs of the subsequent adaptive noise canceller. Then the adaptive noise canceller filters out periodic vibration signals related to the track mode. Finally, the simulation and experiment results show that the designed digital adaptive filter can suppresses basic frequency, second harmonic, third harmonic, and other vibration components on the elastic support beams effectively.

II. SYSTEM MODEL AND ADAPTIVE FILTER ARCHITECTURE

The maglev system with an electromagnet considering the elastic deformation of the track is shown in Fig. 1. Here, where z_m and z_G denote the vertical (direction of OZ) displacements of the electromagnet and the track, respectively, and z is the suspension gap. F and mg denote separately the electromagnetic force and the weight of the electromagnet. u , R and i are the voltage, resistor and current of the electromagnet winding.

Considering the first-order vibration mode of the track, the model of maglev system with flexible track can be presented as following [8]:

$$\begin{cases} z = z_m - z_G \\ (m + M)g - C_1 \frac{i^2}{z^2} = m\ddot{z}_m \\ u = Ri + 2\frac{C_1}{z} \dot{i} - \frac{2C_1 i}{z^2} \dot{z} \\ \ddot{z}_G + 2\eta_1 \omega_1 \dot{z}_G + \omega_1^2 z_G = C_2 \frac{i^2}{z^2} \end{cases}, \quad (1)$$

where M is the mass of carriage, η_1 and ω_1 are the

damping ratio and natural frequency of first-order mode respectively, C_1 , C_2 are the system parameters.

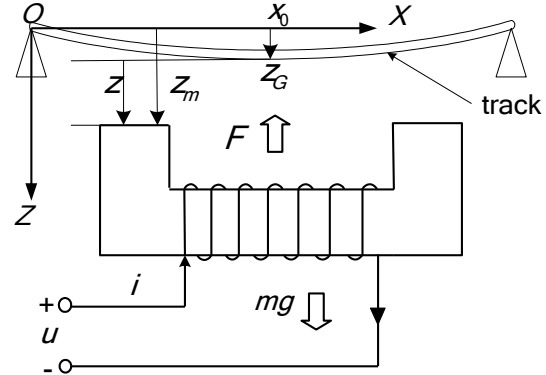


Fig. 1. The maglev system with flexible track.

In order to make the electromagnet suspend at certain air gap z_e , a state feedback control algorithm can be adopted as follows [8]:

$$u = u_e + k_g z + k_v \dot{z} + k_i i, \quad (2)$$

where k_g , k_v , k_i are the control parameters of suspension gap, velocity and current, respectively. v_e is the initial voltage of the electromagnet.

From (8), we can find that the deformation of the elastic track in the control law can't be ignored. As mentioned above, the vibration components related to the track mode can be suppressed by some filter technology.

In this section, an architecture of an adaptive filter for suppressing the vehicle-track coupled vibration with multiple vibration frequencies is presented in Fig. 2. It contains an adaptive self-tuning filter, a narrow-band bandpass filter, and an adaptive noise canceller.

In Fig. 2, the adaptive self-tuning filter is to filter out the wideband signals and noises from the original signal and enhance the strength of the basic wave and various components related to the track vibration mode. The narrow-band bandpass filter is to extract periodical signals related to the track mode for use as reference signals of the adaptive noise filter. Finally, the adaptive noise canceller is to filter out the periodical vibration signals related to the track mode.

The following sections discuss the working principles of the adaptive self-tuning filter and adaptive noise canceller.

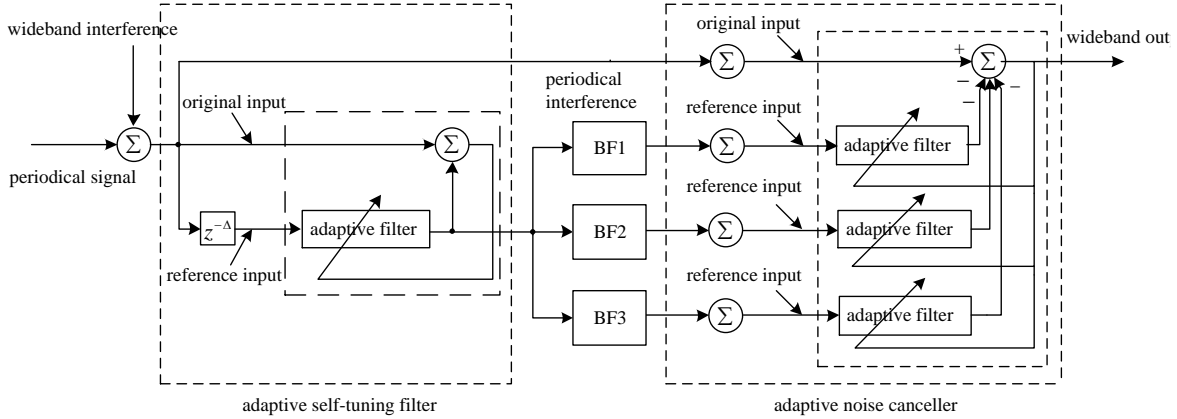


Fig. 2. Architecture of the adaptive filter with multiple central frequencies.

III. DESIGN OF THE ADAPTIVE SELF-TUNING FILTER WITHOUT REFERENCE INPUT

In an actual maglev system, the frequency of time-varying periodical interference in a single gap is variable and unknown. Thus, no related outside reference input signal can be used. In this section, an adaptive self-tuning filter without outside reference input is presented. This filter can extract periodical gap fluctuation signal, including the baseband signal, second harmonic, and third harmonic related to the track vibration mode. Therefore, this filter can be considered a spectral linear enhancer. The structure of the adaptive self-tuning filter is shown in Fig. 3.

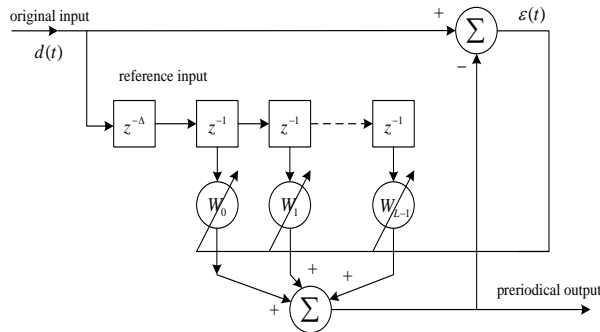


Fig. 3. The adaptive self-tuning filter with original sensor output.

We denote the original sensor signal of the maglev system as following [13]:

$$d(t) = s(t) + n(t) = \sum_{i=1}^M A_i e^{j(\omega_i t + \theta_i)} + n(t), \quad (3)$$

where $s(t)$ is the periodical component, $n(t)$ is the wideband component with stable Gauss white noise. A_i, ω_i, θ_i refer to the amplitude, frequency, and starting

phase of the i_{th} sinusoidal signal, respectively.

We select a proper Δ , such that,

$$E\{n(t)n(t-\Delta)\} = 0. \quad (4)$$

From (4), the broadband signal component $n(t)$ and $n(t-\Delta)$ are decorrelated. However, the components of vibration interference $s(t)$ and $s(t-\Delta)$ are still related to each other because of their periodicity.

If the mean power of noise $n(t)$ is given as $M\delta_0^2$, the mean power of the i_{th} sinusoidal signal is $\delta_i^2 = A_i^2/2$, and its input signal-to-noise ratio is:

$$SNR_i = \frac{\delta_i^2}{\delta_0^2}. \quad (5)$$

Here X represents the vector composed of the signals of all taps in the delay line, and a weight vector represents the adaptive filter with length L . Thus,

$$X^T = [x_0 \ x_1 \ \dots \ x_{L-1}]^T, \quad W^T = [w_0 \ w_1 \ \dots \ w_{L-1}]^T. \quad (6)$$

The output of adaptive tuning filter is given by:

$$y(t) = W^T X = X^T W. \quad (7)$$

The system error signal is expressed as:

$$\varepsilon(t) = d(t) - y(t) = d(t) - W^T X. \quad (8)$$

A common criterion for filter design is minimization of the mean-square error between filter output and expected response, that is,

$$E\{|\varepsilon(t)|^2\} \rightarrow \min. \quad (9)$$

Substituting Eq. (8) into (9), $\bar{d}(t)$ is used to represent the conjugant of $d(t)$, such that we obtain:

$$\begin{aligned} E\{|\varepsilon(t)|^2\} &= E\{[d(t) - W^T X]^2\} \\ &= E\{d(t)\bar{d}(t) - d(t)\bar{W}^T \bar{X} - \bar{d}(t)W^T X \\ &\quad + W^T X \bar{X}^T \bar{W}\} \end{aligned} \quad (10)$$

If $P = E\{d(t)\bar{X}\}$, the autocorrelative matrix of filter tap input X is:

$$R_{X\bar{X}} = E\{X\bar{X}^T\} = E\{XX^H\}, \quad (11)$$

where $X^H = \bar{X}^T$ refers to the conjugate transpose matrix of X . $R_{X\bar{X}}$ is generally a symmetric matrix that is definitely positive.

Eq. (8) can be rewritten as:

$$E\{|\varepsilon(t)|^2\} = E\{d(t)\bar{d}(t) - 2\text{Re}(W^H P) + W^T R_{XX} \bar{W}\}. \quad (12)$$

In the above equation, $\text{Re}(W^H P)$ refers to the real part of $W^H P$.

Based on the LMS (Least mean square) criterion, the optimal weight vector (Wiener solution) of this filter is:

$$W^* = R_{X\bar{X}}^{-1} P. \quad (13)$$

The above equation shows that if this filter aims to adaptively track input signals, the matrix $R_{X\bar{X}}^{-1}$ must be calculated in real-time. To avoid the inconvenience of matrix inversion in real-time signals, we can update the weight vector by using the steepest descent LMS algorithm [13,14].

The expected value of the weight vector can be obtained in the main coordinates if and only if:

$$0 < \mu < \lambda_{\max}^{-1}, \quad (14)$$

where μ is the converging factor refers to a gain constant for controlling adaptive speed and stability, λ_{\max} refers to the maximal eigenvalue of input-related matrix $R_{X\bar{X}}$. The parameter λ_{\max} is not higher than the trace of the input-related matrix $R_{X\bar{X}}$ (the sum of the diagonal elements), and the convergence of the weight vector can be ensured by the following equation:

$$0 < \mu < (\text{tr}R)^{-1}. \quad (15)$$

In the equation above, the diagonal elements of the input-related matrix $R_{X\bar{X}}$ (i.e., the input power) are easier to estimate than the eigenvalue of $R_{X\bar{X}}$ and can easily be used in practice.

In the following section, we deduce the transfer function of the self-tuning filter. This function can be obtained on the basis of the steady impulse response of the filter through discrete Fourier transform.

The steady impulse response function of filter is given by:

$$W_k^i = \sum_{i=1}^N A_i e^{j\omega_i k}, \quad k = 0, 1, 2, \dots, L-1. \quad (16)$$

Thus,

$$\begin{aligned} H(\omega) &= \sum_{k=0}^{L-1} W_k^i e^{-j\omega(\Delta+k)} \\ &= \sum_{k=0}^{L-1} \sum_{i=1}^M A_i e^{j\omega_i k} e^{-j\omega(\Delta+k)} \\ &= \sum_{i=1}^M A_i e^{-j\omega\Delta} \sum_{k=0}^{L-1} e^{j(\omega_i - \omega)k} \\ &= \sum_{i=1}^M A_i e^{-j\omega\Delta} \frac{1 - e^{j(\omega_i - \omega)L}}{1 - e^{j(\omega_i - \omega)}} \end{aligned} \quad (17)$$

If L is very high, no relation exists among M sine waves. Thus,

$$A_i = \frac{e^{j\omega_i \Delta}}{L + \delta_0^2 / \delta_i^2}. \quad (18)$$

The transfer function of the filter is:

$$H(\omega) = \sum_{i=1}^M \frac{e^{j(\omega_i - \omega)\Delta}}{L + \delta_0^2 / \delta_i^2} \frac{1 - e^{j(\omega_i - \omega)L}}{1 - e^{j(\omega_i - \omega)}}. \quad (19)$$

Equation (19) shows that this self-tuning filter is equivalent to the sum of M bandpass filters with central frequency ω_i .

The above equation shows that the amplitude/frequency response of the i_{th} filter is:

$$H_i(\omega) = \frac{1}{L + \delta_0^2 / \delta_i^2} \left| \frac{1 - e^{j(\omega_i - \omega)L}}{1 - e^{j(\omega_i - \omega)}} \right|. \quad (20)$$

If $\omega \rightarrow \omega_i$, $\frac{1 - e^{j(\omega_i - \omega)L}}{1 - e^{j(\omega_i - \omega)}}$ in the above equation refers to $\frac{0}{0}$ type, and $\frac{(1 - e^{j(\omega_i - \omega)L})'}{(1 - e^{j(\omega_i - \omega)})'} = L$. Thus, the maximum amplitude-frequency response of the i_{th} filter is:

$$H_i(\omega)_{\max} = \frac{L}{L + \delta_0^2 / \delta_i^2} = \frac{L(\text{SNR})_i}{1 + L(\text{SNR})_i}. \quad (21)$$

To verify the performance of the self-tuning filter, the input signal is given as $x(t) = s(t) + n(t)$, with the periodical signal being $s(t) = \sin(2\pi \cdot 50 \cdot t) + 0.7\sin(2\pi \cdot 100 \cdot t) + 0.4\sin(2\pi \cdot 150 \cdot t) + 1$. The wideband signal of random noise is $n(t) = 0.56\text{randn}(1, N)$. The sampling frequency is 2000 Hz. The order of the self-tuning filter is 96, the sample data comprise 10000 points, and $\mu = 0.002$. When the delay time is set to $\Delta = 256$, the spectrograms of the input and output signal can be obtained as shown in Fig. 4.

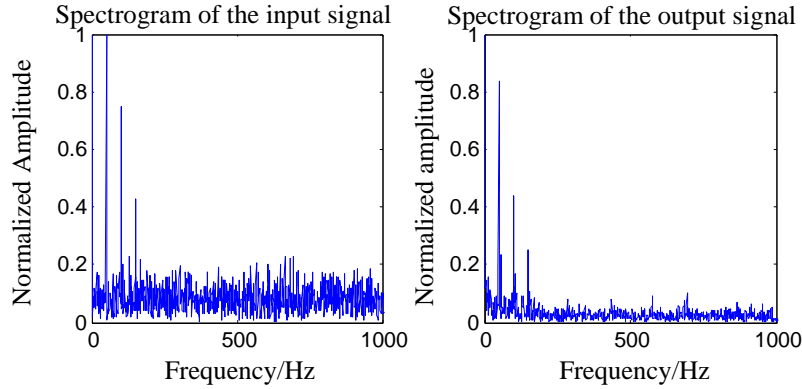


Fig. 4. Spectrogram of input and output signal of self-tuning filter with a delay time 256.

Figure 4 shows that when the delay time is 256, the spectral lines of the output at 50 Hz, 100 Hz, and 150 Hz are enhanced and the wideband signals with noise is weakened. Then we can adopt the self-tuning filter to filter out the wideband signals and noises from the original signal, and enhance the strength of the vibration components related to the track mode for the maglev system.

IV. DESIGN OF THE ADAPTIVE NOISE CANCELLER WITH MULTIPLE REFERENCE INPUTS

We suppose that the original input signal of the maglev system is arbitrary, that is, it can be random, determinate, continuous, or transient. When a vehicle-track coupled vibration occurs, it may even be a combination of the basic wave and various components related to the track vibration mode.

The architecture of the adaptive noise canceller with multiple frequencies is presented in Fig. 5. The rationality of the algorithm is discussed below.

The reference input signal with any single frequency can be denoted as:

$$x_i(t) = A_i \cos(2\pi f_i t + \varphi_i), i = 1, 2, 3. \quad (22)$$

In Fig. 5, for the first reference input signal with the single frequency, the input of the first weight can be directly obtained from reference input, and the input of the second weight is obtained after a 90-degree phase shift of the first weight input, that is,

$$x_{i1k} = A_i \cos(k\omega_i t + \varphi_i), x_{i2k} = A_i \sin(k\omega_i t + \varphi_i), \quad (23)$$

where T refers to the sampling period and $\omega_i = 2\pi f_i T$.

Weight is iterated by using the LMS algorithm [13,15]. The flowchart of the adaptive noise canceller is presented in Fig. 6.

For simplicity, the feedback loop from G to B is disconnected in Fig. 6 during analysis of the open-loop transmission characteristics of the adaptive noise canceller, that is, the isolated impulse response from error C to G. We suppose that a discrete unit impulse function is inputted in C at $k = m$, such that,

$$\varepsilon_{ik} = \delta(k - m). \quad (24)$$

To reach D in the upper branch passing through a multiplier at I is a signal composed of multiple sinusoidal functions such that the system is determined to be a time-varying system. The output response is:

$$h_{i1} = \begin{cases} A_i \cos(m\omega_i t + \varphi_i), & k = m \\ 0, & k \neq m \end{cases}. \quad (25)$$

A digital integrator exists from D to E with the transfer function $2\mu/(z-1)$. The impulse response is:

$$h_{i2} = 2\mu u(k-1), \quad (26)$$

where $u(k)$ refers to the discrete unit step function. The parameters h_{i1}, h_{i2} are used for the convolution operation, and the output response at E is:

$$\omega_{i1k} = h_{i1} \otimes h_{i2} = 2\mu A_i \cos(m\omega_i + \varphi_i). \quad (27)$$

In the above equation, $k \geq m+1$. This function is multiplied by the multiplication factor x_{i1k} at H such that the output response at F is:

$$y_{i1k} = 2\mu u(k-m-1) A_i \cos(m\omega_i + \varphi_i) \cdot A_i \cos(k\omega_i + \varphi_i). \quad (28)$$

Similarly, the output response at J is:

$$y_{i2k} = 2\mu u(k-m-1) A_i \sin(m\omega_i + \varphi_i) \cdot A_i \sin(k\omega_i + \varphi_i). \quad (29)$$

By combining the two equations above, the response at the output end G of the filter can be obtained as:

$$y_{ik} = y_{i1k} + y_{i2k} = 2\mu u(k-m-1) A_i^2 \cos[(m-k)\omega_i]. \quad (30)$$

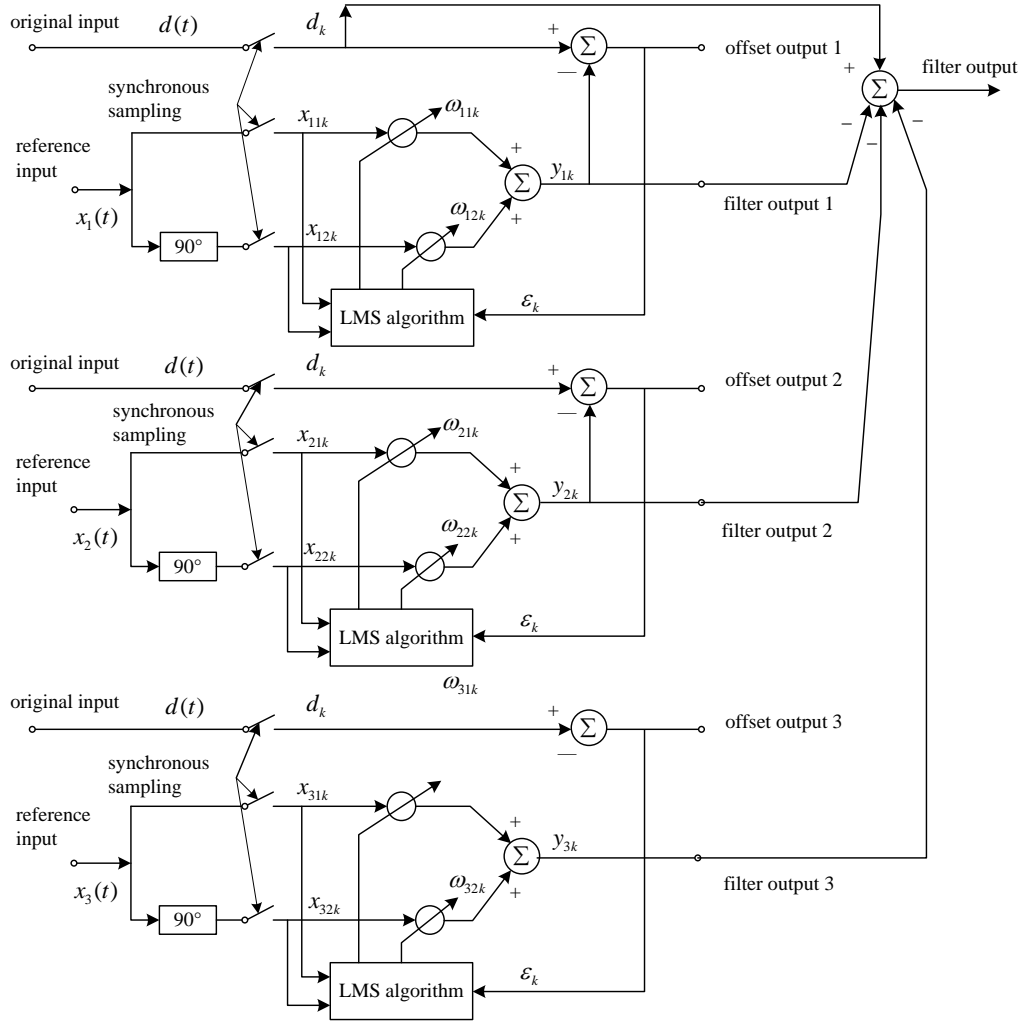


Fig. 5. Adaptive noise canceller with multiple reference frequency.

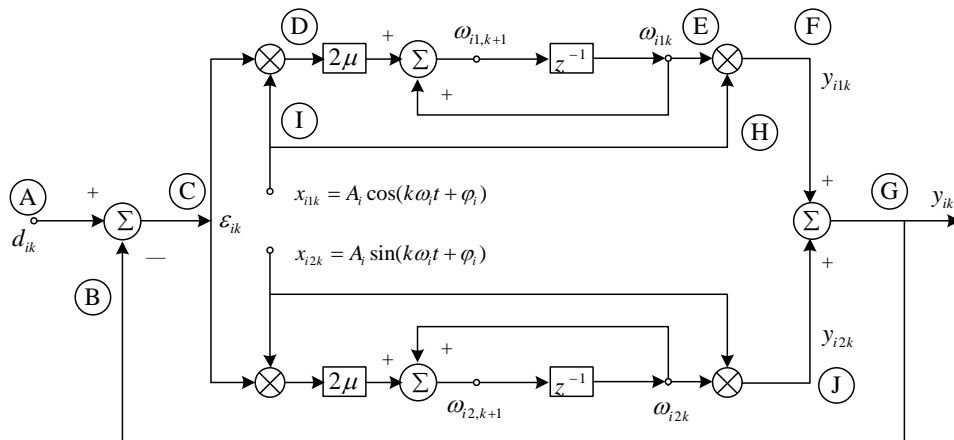


Fig. 6. Signal transmission flowchart of LMS algorithm.

The equation above is a function related to $k-m$. If the impulse moment m is taken as 0, the open-loop

impulse response from C to G can be obtained as:

$$y_{ik} = y_{i1k} + y_{i2k} = 2\mu u(k-1)A_i^2 \cos(k\omega_i). \quad (31)$$

The transfer function from C to G in this channel is the z conversion of the above equation, that is,

$$G(z) = 2\mu A_i^2 \frac{z \cos \omega_i - 1}{z^2 - 2z \cos \omega_i + 1}. \quad (32)$$

In fact, the above-mentioned open-loop system is an unsteady system. Now, we connect the feedback loop from G to B to be closed. Thus, we can obtain a closed-loop transfer function from original input A to noise cancel output C:

$$H(z) = \frac{1}{1+G(z)} = \frac{z^2 - 2z \cos \omega_i + 1}{z^2 - 2(1 - \mu A_i^2)z \cos \omega_i + 1 - 2\mu A_i^2}. \quad (33)$$

The above equation is a canceller with a single frequency. A zero point is found at the reference frequency f_i and accurately located at $z = e^{\pm j\omega_i}$ inside the unit circle in the Z plane. The poles are located at:

$$z_{ip} = (1 - \mu A_i^2) \cos \omega_i \pm j[(1 - 2\mu A_i^2) - (1 - \mu A_i^2)^2 \cos^2 \omega_i]^{0.5}. \quad (34)$$

Two conjugate poles may be easily found inside the unit circle. Thus, the above closed-loop system is stable. Based on the above equation, the module of this pole is $(1 - 2\mu A_i^2)^{0.5}$, and its angle is:

$$\begin{aligned} z_{ip} &= (1 - 2\mu A_i^2)^{\pm j0.5 \arccos[(1 - \mu A_i^2)(1 - 2\mu A_i^2)^{-0.5} \cos \omega_i]} \\ &= (1 - \mu A_i^2)^{\pm j \arccos[(1 - \mu A_i^2)(1 - 2\mu A_i^2)^{-0.5} \cos \omega_i]} \end{aligned} \quad (35)$$

For a slow adaptive process, μA_i^2 in the above equation is very small, and the factor in the exponential term can be arranged as:

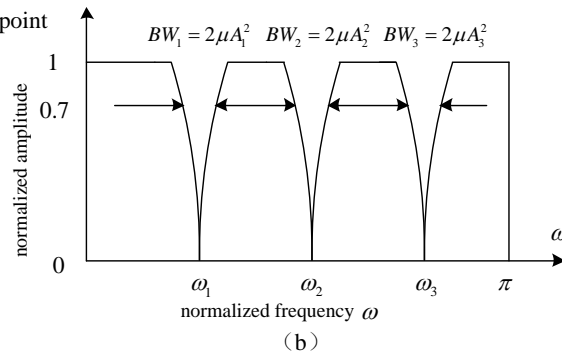
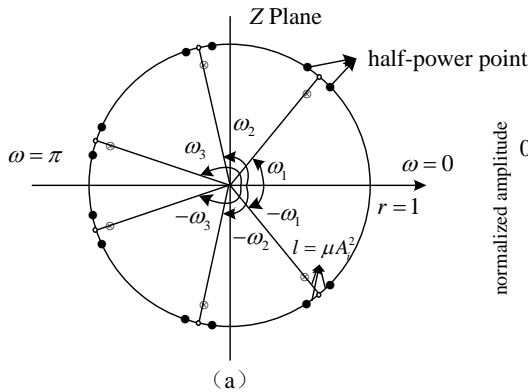


Fig. 7. The characteristics of the adaptive noise canceller with many reference frequencies.

Figure 7 clearly shows that when the reference frequency is slowly changed, the adaptive notch process can be adjusted to the phase relation required by cancellation.

Here, the zero point of the transfer function of the whole filter is on the unit circle. However, the distribution of poles is not completely regular. If the sum of various harmonic signals that serve as output from the

$$\begin{aligned} \frac{1 - \mu A_i^2}{(1 - 2\mu A_i^2)^{0.5}} &= \left[\frac{1 - 2\mu A_i^2 + \mu^2 A_i^4}{1 - 2\mu A_i^2} \right]^{0.5} \\ &= [1 + \mu^2 A_i^4 + \dots]^{0.5} = 1 + \frac{\mu^2 A_i^4}{2} + \dots \end{aligned} \quad (36)$$

The equation above suggests that the pole can be approximately represented as:

$$z_{ip} = (1 - \mu A_i^2)^{\pm j\omega_0}. \quad (37)$$

Therefore, the angle of the pole is almost equal to that of the zero point under actual circumstances. The pole points and zero points of the transfer function are shown in Fig. 7 (a). The zero points are on the unit circle, so the transfer function is infinitely deep at $\omega = \omega_0$. The sharpness of the notch is determined by the distance μA_i^2 from pole to zero. The distance between half-power points along the unit circle is defined as the arc length, that is, the bandwidth of the notch filter. We find that [14,15]:

$$BW = 2\mu A_i^2 \text{ rad} / s = \frac{\mu A_i^2}{\pi T} \text{ Hz}. \quad (38)$$

Notch sharpness is represented by a quality factor, which is defined as the ratio of central frequency to band width, that is,

$$Q = \frac{\omega_0}{2\mu A_i^2}. \quad (39)$$

Thus, when the reference input contains multiple sine wave signals, the adaptive noise cancelling process is equal to a filter with many central notch frequencies, as shown in Fig. 7 (b).

adaptive filter is regarded as the reference signal, the subsequent adaptive process is not necessarily convergent. For example, the sum of three sine wave signals is used as the reference input and the Matlab software is adopted for numerical analysis. We find out that improperly set parameters can easily cause the adaptive noise canceller to become unstable. Analysis shows that the adaptive noise canceller is actually an IIR filter and the pole

is close to the unit circle, so improper coefficient quantization is easily to cause the filter to be unstable. Also, the high-order IIR filtering process is often unstable, so we should properly set the gain of each link to prevent the filter from experiencing divergence in the cascade form of two-order IIR filters [16,17].

To verify the performance of the adaptive filter, we set the input signal as $x(t) = s_1(t) + s_2(t) + s_3(t) + n(t)$, adopt a signal-to-noise ratio of 10 dB, and assign the three periodical reference signals as $s_1(t) = \sin(2\pi \cdot 50 \cdot t)$, $s_2(t) = 0.7\sin(2\pi \cdot 100 \cdot t)$, $s_3(t) = 0.4\sin(2\pi \cdot 150 \cdot t)$. Here, the wideband signal with random noise is $n(t) = 0.56\text{randn}(1, N) + 1$. The order of the three adaptive noise cancellers is 2. The amplitude-phase characteristic curves of the adaptive noise canceller are shown in Fig. 8. When the frequencies of three sine wave reference signals are known, the amplitude-frequency curves for the adaptive noise canceller described above are similar to the filter with three notches.

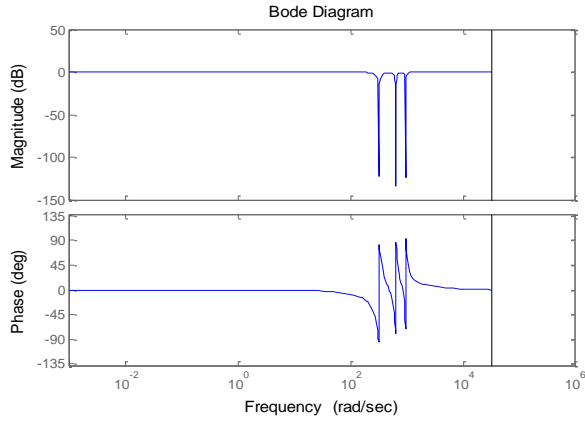


Fig. 8. Amplitude-frequency characteristic curves of the adaptive noise canceller.

V. EXPERIMENTAL VERIFICATION

Engineering tests show that when the vehicle is suspended statically on the steel girders, cantilever beams, turnouts or running at a speed lower than 5 km/h, the vehicle-track coupled vibration is prone to occur. There are 60 suspension control systems in a low-speed maglev train, and each control system needs to collect three displacement signals, one acceleration signal and one current signal in real-time. Because of the massive real-time sensor data from the whole train system, we use a high-speed CAN bus equipment to collect these sensor data from all 60 controllers. Here, each controller sends its own sensor data including displacement, acceleration and current to the CAN bus, and the train operation control equipment store the real-time data of the sensors on-line. The sampling frequency of these data is 2500 Hz and it is convenient for on-line fault diagnosis or off-line

data analysis for the maglev train.

Figure 9 is the curve of the sensors of a vehicle-track coupled vibration for 5 seconds, including the vehicle's suspending process and low-speed operation process.

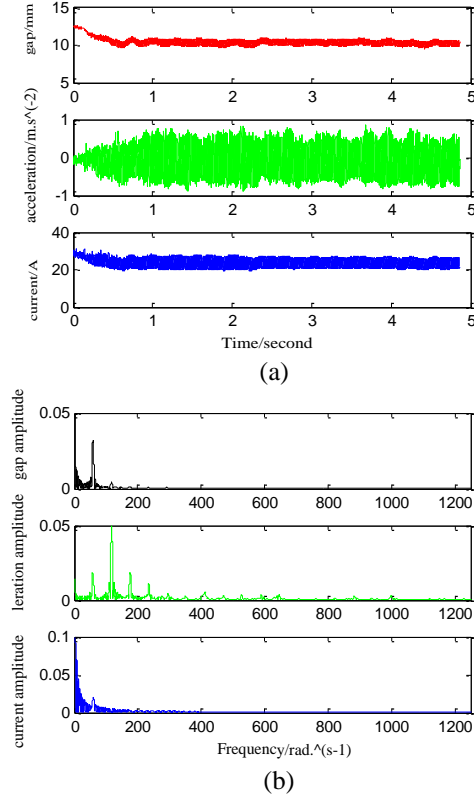


Fig. 9. Sensor output curves and spectrum of a vehicle-track coupled vibration.

From Fig. 9 (a), when a vehicle-track coupled vibration occurs, the gap fluctuation is more than 0.5 mm, the acceleration fluctuation is higher than 0.6m/s^2 , and the current fluctuation is higher than 7.7A. In Fig. 9 (b), it contains obvious periodical signals such as fundamental frequency 58Hz, second harmonic 117Hz and third harmonic 174Hz.

When the vehicle is suspended on the same elastic track, we introduce the adaptive filter to the control system, and acquire the curves of the signals of gap, acceleration, and current sensors as shown in Fig. 10.

Figure 10 (a) shows that when the adaptive filter with multiple central frequencies is applied to the system, the vehicle-track coupled vibration no longer occurs while the vehicle is levitated statically in the garage. The gap fluctuation is no higher than 0.3 mm, the acceleration fluctuation is no higher than 0.06m/s^2 , and the current fluctuation is no higher than 0.7A. In Fig. 10 (b), there are no obvious periodical signal is observed from the gap, acceleration, or current signals. Starting

from 35 s, the vehicle enters the landing process and lands on the track at 37 s. The current of the magnet drops to 0 A at 38 s. It shows that coupled vibration has been suppressed effectively.

In the same way, while the vehicle is levitated statically or runs at a low-speed on other elastic beams, there is no obvious periodical signal related to the track mode. It indicates that that the adaptive filter without frequency measurement can effectively suppress the vehicle-track coupled vibration for different elastic tracks to a certain extent.

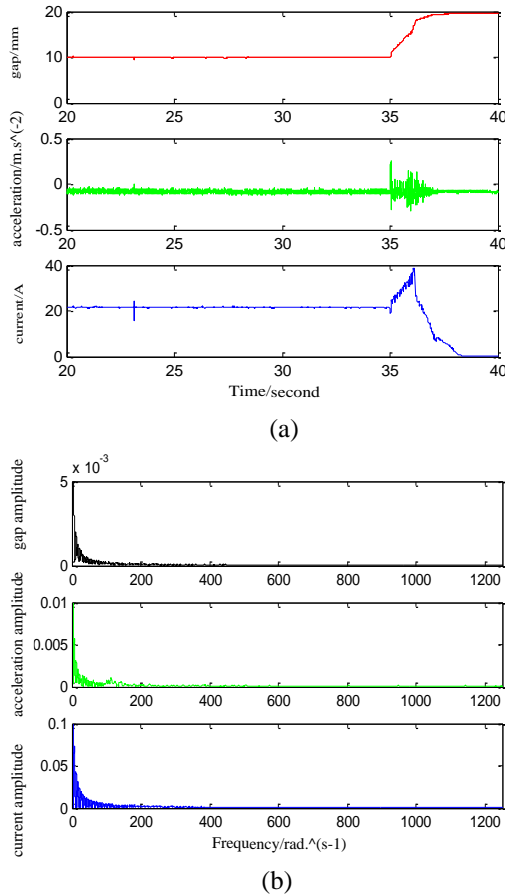


Fig. 10. Sensor output curves and spectrum of the adaptive filter with multiple central frequencies.

VI. CONCLUSION

This study aims to solve the vehicle-track coupled vibration problem that occurs during levitation or low-speed running of the maglev system from the perspective of signal processing. The fundamental waves, higher order harmonics, and other components related to the mode of track vibrations are often found in the gap, acceleration, and current sensors. An adaptive filter is designed to suppress these vibration components and improve the ride comfort for the passengers.

The adaptive filter with multiple central frequencies

doesn't need outside reference input signals. This filter effectively filters out the wideband signals and noises from the original signal and enhances the strength of the basic wave and various components related to the track vibration mode.

The narrow-band bandpass filter extracts the periodical signals related to the track mode for use as reference signals of the adaptive noise filter. And the adaptive noise canceller filters out the periodical vibration signals related to the track mode. It should be noted that the self-tuning process must be convergent.

Experimental results show that the designed digital filter effectively suppresses vehicle-track coupled vibration on different elastic beams. In the next step, we will further improve the stability proof of the algorithm.

ACKNOWLEDEMENT

This work was supported by the National Natural Science Foundation of China (61304036), and China Postdoctoral Science Foundation (2014M562651, 2015T81132), the Natural Science Foundation of Hunan Province, China (2015JJ3019). The authors wish to thank the anonymous reviewers for their efforts in providing the constructive comments that have helped to significantly enhance the quality of this paper.

REFERENCES

- [1] H. W. Lee, K. C. Kim, and J. Lee, "Review of maglev train technologies," *IEEE Trans. on Magnetics*, vol. 42, pp. 1917-1925, 2006.
- [2] M. Nagai, "The control of magnetic suspension to suppress the self-excited vibration of a flexible track," *Jpn. Soc. Mech. Eng.*, vol. 30, no. 260, pp. 365-366, 1987.
- [3] L. H. She, Z. Z. Zhang, D. S. Zou, et al., "Multi-state feedback control strategy for maglev elastic vehicle-guideway-coupled system," *Advanced Science Letters*, vol. 5, no. 2, pp. 587-592, 2012.
- [4] H. P. Wang, J. Li, and K. Zhang, "Stability and Hopf bifurcation of the maglev system with delayed speed feedback control," *Acta Automatica Sinica*, vol. 33, no. 8, pp. 829-834, 2007.
- [5] L. L. Zhang, L. H. Huang, and Z. Z. Zhang, "Stability and Hopf bifurcation of the maglev system with delayed position and speed feedback control," *Nonlinear Dyn.*, vol. 57, no. 1-2, pp. 197-207, 2009.
- [6] L. L. Zhang, L. H. Huang, and Z. Z. Zhang, "Hopf bifurcation of the maglev time-delay feedback system via pseudo-oscillator analysis," *Mathematical and Computer Modelling*, vol. 52, no. 5-6, pp. 667-673, 2010.
- [7] D. S. Zou, L. H. She, Z. Z. Zhang, and W. S. Chang, "Maglev system controller design based on the feedback linearization methods," *2008 IEEE International Conference on Information and Automation*,

- Zhangjiajie, China, 2008.
- [8] Z. Z. Zhang and L. L. Zhang, "Hopf bifurcation of time-delayed feedback control for maglev system with flexible track," *Applied Mathematics and Computation*, vol. 219, no. 11, pp. 6106-6112, 2013.
- [9] D. Zhang, Y. G. Li, H. K. Liu, et al., "Restrain the effects of vehicle-track dynamic interaction: bandstop filter method," *Maglev2008 Proceedings*, 2008.
- [10] H. Li and R. M. Goodall, "Linear and non-linear skyhook damping control laws for active railway suspensions," *Control Eng. Pract.*, vol. 7, no. 7, pp. 843-850, 1999.
- [11] Q. J. Han, "From PID to active disturbance rejection control," *IEEE Trans. Ind. Electron.*, vol. 56, no. 3, pp. 900-906, 2009.
- [12] L. L. Zhang, Z. Z. Zhang, and L. H. Huang, "Hybrid nonlinear differentiator design for permanent-electromagnetic suspension maglev system," *Signal Processing*, vol. 6, no. 6, pp. 559-567, 2012.
- [13] S. Haykin, *Adaptive Filter Theory*. 5th Edition, Pearson Education Inc., 2013.
- [14] Z. W. Liu, R. S. Chen, and J. Q. Chen, "Using adaptive cross approximation for efficient calculation of monostatic scattering with multiple incident angles," *The Applied Computational Electromagnetics Society*, vol. 26, pp. 325-333, Apr. 2011.
- [15] S. Xue, Z. Q. Long, N. He, and W. S. Chang, "A high precision position sensor design and its signal processing algorithm for a maglev train," *Sensors*, vol. 12, pp. 5225-5245, 2012.
- [16] L. L. Zhang and J. H. Huang, "Stability analysis for a flywheel supported on magnetic bearings with delayed feedback control," *The Applied Computational Electromagnetics Society*, vol. 32, no. 8, pp. 642-649, 2017.
- [17] L. Y. Xiang, S. G. Zuo, and L. C. He, "Electric vehicles to reduce vibration caused by the radial force," *The Applied Computational Electromagnetics Society*, vol. 29, pp. 340-350, Sep. 2014.



Zhizhou Zhang received the B.S. degree in Automation from Northeastern University, China, in 2004. He received the M.S. and Ph.D. degrees in Control Science and Engineering from National University of Defense Technology, China, in 2006 and 2011. Since 2011, he works at the College of Aerospace Science, National University of Defense Technology. His research interest is maglev control.